

# **An Intuitive Approach to Orbital Deprojection: Analyzing the Orbit of S2 in the Sagittarius A\* Cluster**

**Nicholas Holquist**

Under the supervision of

Mark Whittle

University of Virginia

Department of Astronomy

May 2025

This thesis is submitted in  
Partial Completion of the Requirements for the  
B.S. Astronomy-Physics Major

## Abstract

The orbit of the star S2 around the supermassive black hole Sgr A\* at the center of the Milky Way provides one of the most compelling observational laboratories for testing gravitational dynamics. This project develops an intuitive and educationally accessible yet physically rigorous framework for modeling the orbit of S2 using publicly available astrometric and spectroscopic data, specifically the dataset compiled by Gillessen et al. (2017) from observations with the ESO Very Large Telescope. The methodology enables students—from secondary school to undergraduate levels—to derive the six classical orbital elements describing S2's motion and to estimate the mass of Sgr A\* using Keplerian dynamics. Additionally, radial velocity data are used to validate the orbital solution and estimate the distance to the Galactic Center. Beyond the technical objectives, the project aims to foster intuitive understanding and scientific curiosity by bridging modern observational data with classical celestial mechanics. The framework is implemented in both a slider-based Desmos interface for introductory engagement and an Excel-based workflow for more advanced analysis. This project thus serves not only as a pedagogical tool but also as a case study in democratizing access to high-precision astrophysical datasets and methods.

*Keywords: orbital deprojection, S2, Sgr A\**

# I. Introduction

## 1.1 Scientific Motivation

Black holes are our most striking window into new physics. They are where our best theories collide, where paradoxes erupt, and where the seams in our understanding of the universe begin to fray. In the extreme environments they govern, where spacetime contorts and quantum effects boil to the surface, black holes compel us to seek a deeper, unified description of reality—one that transcends the patchwork of general relativity and quantum mechanics. They are not just gravitational anomalies; they are portals to the next revolution in physics.

The journey to understanding black holes began in earnest over half a century ago, when Roger Penrose demonstrated that the formation of singularities is not a quirk of symmetry, but a generic outcome of gravitational collapse. His 1965 theorem, one of the most profound results in the history of physics, showed that under reasonable physical conditions, a collapsing mass inevitably leads to the formation of a region from which nothing, not even light, can escape. In other words, black holes are not just mathematical oddities within Einstein's equations—they are inevitable. Penrose's insight, for which he would win the Nobel Prize decades later, gave theoretical legitimacy to the idea that black holes are a real and unavoidable feature of our universe (Nobel Committee for Physics 2020).

Yet theory alone could not satisfy the scientific appetite, and the cosmos does not always yield its deepest secrets willingly. Observational evidence remained elusive, and for decades black holes were ghostly conjectures, haunting the equations of relativity but unseen. That changed dramatically with the discovery of quasars in the 1960s—some of the brightest, most distant objects in the universe, whose radiative output dwarfs that of entire galaxies. The only engine capable of such luminosity, it was soon realized, was accretion onto a supermassive black hole. From that moment, the direct detection of a black hole became a scientific holy grail. Quasars were beacons from the early universe, but they were too far away to resolve their inner workings. If we could find a nearby example, we could make observations not merely by inference but through its gravitational dominion. The search intensified and our gaze turned inward to the core of our own galaxy. At the heart of the Milky Way lies Sagittarius A\* (Sgr A\*), a compact radio source that would become one of the most scrutinized objects in the search for a black hole.

Yet peering into the core of our own Milky Way is no simple endeavor. The Galactic Center, while just 26,000 light-years away—a mere whisper on the cosmic scale—is cloaked in veils of gas and dust that thwart our optical vision. The interstellar medium between Earth and Sgr A\* absorbs and scatters visible light so thoroughly that the entire region appears nearly opaque to even our most powerful optical telescopes. In the infrared, the story changes. Longer-wavelength photons slip more freely through the interstellar murk, allowing infrared-sensitive instruments like those on the Very Large Telescope (VLT) and the Keck Observatory to peel back the cosmic curtain. Even so, the view is not pristine: a tangled web of dust filaments, molecular clouds, and turbulent flows continues to obscure and complicate the path of the light we receive.

The Galactic Center is not just hidden, it is a cauldron of incredible complexity, teeming with phenomena that light up the electromagnetic spectrum: in the radio regime, we see non-thermal synchrotron emission

tracing relativistic electrons spiraling around magnetic fields; in the X-ray regime, orbiting observatories like Chandra have revealed flares and shocks, some likely originating from accretion events near the black hole's event horizon; and in the gamma regime, the Fermi Gamma-ray Space Telescope revealed two immense gamma-ray-emitting lobes ballooning above and below the Galactic plane—now known as the Fermi Bubbles. These features span tens of thousands of light-years and may be the lingering echo of an ancient outburst from Sgr A\*, perhaps a long-dead active galactic nucleus (AGN) phase or the cumulative effect of starburst-driven winds.

Against this energetic backdrop, the question of *what exactly* resides at the very center becomes one of both observational rigor and theoretical necessity. It is not enough to infer the presence of a massive object—we must show that the object's mass is confined within a sufficiently small radius that no other known phenomenon can account for it. This is the essence of the black hole argument. The mass alone does not make the case. It is the *density* that crosses the threshold into inevitability.

In professional studies attempting to distinguish black holes from dense star clusters or exotic compact object ensembles, the critical metric is a plot of enclosed mass versus radius. Only when we can show that millions of solar masses lie within a region no larger than the scale of our solar system—tens of astronomical units—can we rule out all alternatives but a black hole.

The key to this extraordinary conclusion lies in the dance of stars around the Galactic Center. Two independent research groups—one led by Reinhard Genzel at the Max Planck Institute for Extraterrestrial Physics (MPE), and the other by Andrea Ghez at the University of California, Los Angeles (UCLA)—painstakingly charted these stellar orbits over decades. Their work, centered on the star known as S2, was recognized with the 2020 Nobel Prize in Physics (Nobel Committee for Physics 2020).

By observing its position on the plane of the sky over time, we can obtain its orbital period directly. With geometry, we can deproject the orbit from our line of sight to reconstruct the true three-dimensional path in the orbital plane. This yields the semi-major axis of the orbit. Then, Kepler's Third Law allows us to determine the enclosed mass.

By mapping the orbits of several stars and examining their radial velocities via Doppler shifts, these researchers were able to build a full dynamical model of the central mass distribution and found that all stellar orbits point to a single, compact, and invisible mass at the core. This, coupled with the shadow image captured by the Event Horizon Telescope, seals the conclusion: Sgr A\* is a supermassive black hole.

## 1.2 Objective

This project aimed to develop a simple, physically intuitive, and technically feasible method for students as early as middle school to replicate key aspects of the analysis done by professional astronomers on the orbit of S2 around Sgr A\*. Specifically, the method enables students to use astrometric data of S2's orbit around the Galactic Center to extract the six classical orbital elements that fully define a Keplerian orbit: semi-major axis, eccentricity, inclination, longitude of the ascending node, argument of periapsis, and time of periapsis passage.

With these elements in hand and the period of the orbit, students can not only model the three-dimensional geometry of S2's orbit but also, through a direct application of Kepler's Third Law, estimate the mass of the central supermassive black hole—reproducing one of the crowning achievements of modern astronomy using first principles. Additionally, the method enables students to use Doppler velocity data of S2's motion along our line of sight to confirm this orbit solution and estimate the distance to the Galactic Center.

## II. Dataset and Observational Context

This project utilizes the astrometric and spectroscopic dataset presented in Table 5 of Gillessen et al. (2017), which provides a long-term monitoring record of the star S2 orbiting the supermassive black hole Sgr A\* at the center of the Milky Way. These data, spanning over two decades, form one of the most complete and precise datasets available for a single stellar orbit in a relativistic gravitational field and have been foundational in establishing the compact mass at the Galactic Center as a black hole.

The dataset contains two primary observables: sky-projected positions of S2 in right ascension ( $\Delta\alpha$ ) and declination ( $\Delta\delta$ ), and line-of-sight radial velocities derived from Doppler shifts. The astrometric measurements are expressed in milliarcseconds (mas) relative to a reference frame centered on Sgr A\*, and the velocity data are given in kilometers per second (km/s). Each observation is timestamped in Julian years, allowing for a temporal reconstruction of the star's orbital motion. The cadence and density of the data are sufficient to constrain all six classical orbital elements and the period of S2's orbit with high precision, as well as to infer properties of the central mass, including its mass and the distance to the Galactic Center,  $R_0$ .

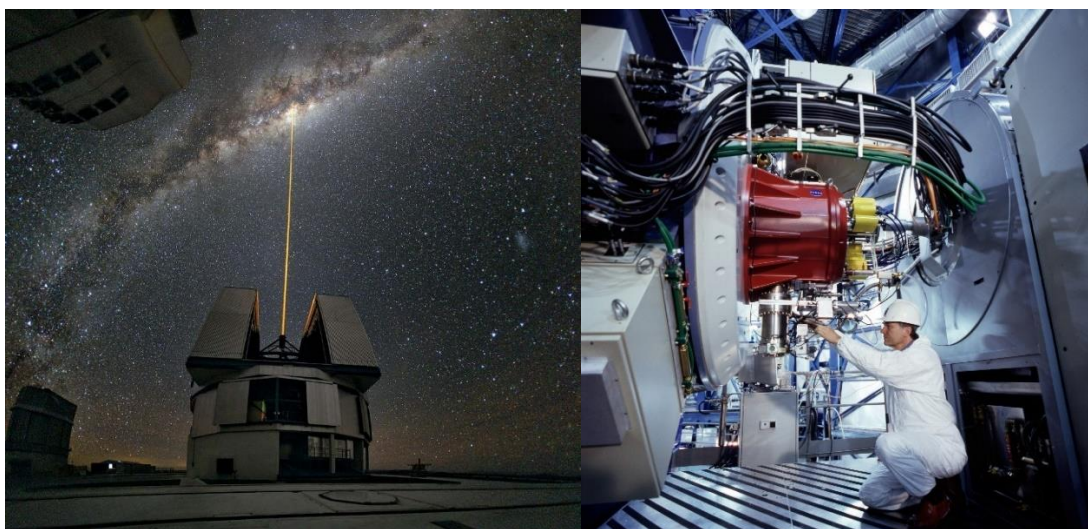


**Figure 1** (Left) Yepun telescope, part of the European Southern Observatory's (ESO's) Very Large Telescope (VLT), observing the centre of the Milky Way, using the laser guide star facility. Image credit: Encyclopædia Britannica (2011), <https://www.britannica.com/topic/Very-Large-Telescope#/media/1/753079/164803>.

**Figure 2** (Right) An engineer adjusts the NAOS-CONICA adaptive optics instrument on the Very Large Telescope (VLT), a system critical for achieving diffraction-limited resolution in near-infrared observations of the Galactic Center. Image credit: ESO (2002), <https://www.eso.org/public/belgium-fr/images/vlt-naos-conica1/>.

The observations were obtained exclusively using instrumentation at the European Southern Observatory's Very Large Telescope (VLT) on Cerro Paranal, Chile. Astrometric data were acquired using the NAOS-CONICA (NACO) adaptive optics imager operating in the near-infrared K-band ( $\lambda \approx 2.2 \mu\text{m}$ ). NACO employs a curvature sensor-based adaptive optics system (NAOS) to correct atmospheric wavefront distortions in real time, enabling angular resolutions approaching the diffraction limit of the 8.2-meter unit telescopes. The need for adaptive optics is dictated by the fact that S2's entire orbit — roughly 0.2 arcseconds in semi-major axis — lies well within the typical atmospheric seeing disk ( $\sim 0.5$ – $1.0''$ ). Without AO correction, the individual positions of S2 and nearby sources would be indistinguishable, and orbital solutions would be impossible to constrain.



*Figure 3 SINFONI—a near-infrared integral field spectrograph—at the integration lab at the ESO Headquarters in Garching in 2004. Image credit: ESO (2004), <https://www.eso.org/public/belgium-fr/images/sinfoni-int-lab-hq2-03-04/>*

Spectroscopic measurements were obtained using SINFONI (Spectrograph for INtegral Field Observations in the Near Infrared), an AO-assisted integral field spectrograph. SINFONI provides three-dimensional data cubes (two spatial, one spectral) in the K-band, making it well-suited for extracting precise Doppler shifts from hydrogen Brackett- $\gamma$  ( $\text{Br}\gamma$ ) absorption lines, even in crowded fields and high-background regions such as the Galactic Center. Together, NACO and SINFONI provide complementary astrometric and kinematic measurements that are essential for orbit determination.

It is worth noting that the Galactic Center region suffers from extreme optical extinction ( $A_v \approx 30$  magnitudes) due to intervening dust, which renders the stellar population invisible at optical wavelengths. However, the extinction in the K-band is reduced to  $A_k \approx 2.5$  magnitudes, enabling infrared instruments to penetrate the obscuring material. Even so, the field remains

complex, with highly variable extinction on small angular scales, bright thermal dust emission, and contamination from both evolved late-type stars and young massive stars.

S2 itself is an early-type main-sequence B star (spectral type B0–2.5 V), which is unusually young ( $< 10$  million years) for its location in the tidal field near Sgr A\*. Its presence raises questions about star formation and dynamical migration in the central parsec. Nonetheless, due to its short orbital period (approximately 16 years), high eccentricity (approximately 0.88), and proximity to the black hole (pericenter distance approximately 120 AU), S2 is the single most important dynamical tracer for determining the mass and compactness of Sgr A\*. The availability of both astrometric and spectroscopic measurements throughout its orbit, particularly near pericenter, makes it an ideal test case for our analyses.

### III. Orbital Deprojection Approach

#### 3.1 Analysis in the Sky Plane

We adopt a right-handed Cartesian coordinate system centered on Sgr A\* at the origin, with the x-axis aligned with right ascension (RA) and the y-axis with declination (Dec). North lies along the +y-direction, and East along the +x-direction—opposite the standard astronomical convention—to facilitate interpretation by students and compatibility with popular plotting software that lacks axis inversion capability. The +z-axis points along the line of sight toward the observer. All positions are measured in milli-arcseconds (mas); at a distance of 8.2 kpc, 1 mas corresponds to 8.2 au.

The first step is to plot the astrometric data to characterize the star's apparent motion on the sky. By analyzing this motion, we aim to deconstruct the star's true three-dimensional orbit.

The projected orbit spans approximately 200 mas (0.2 arcseconds). For context, this is comparable to resolving a U.S. quarter from over 15 miles away. The astrometric precision, on the order of  $\pm 0.4$  mas, corresponds to about half the diameter of a human pupil in daylight ( $\sim 1.2$  mm). These measurements are remarkably precise. Given the Galactic Center's distance of 8.2 kpc, 1 mas corresponds to 8.2 au. Thus, the projected orbital size of 200 mas translates to a physical size of roughly 1600 au. For scale, Neptune's orbit, with a diameter of approximately 60 au, subtends only about 7.2 mas at this distance. The periastron distance of the star's orbit is about 10 mas, or 80 au—equivalent to roughly 10 light-hours from Sgr A\*.

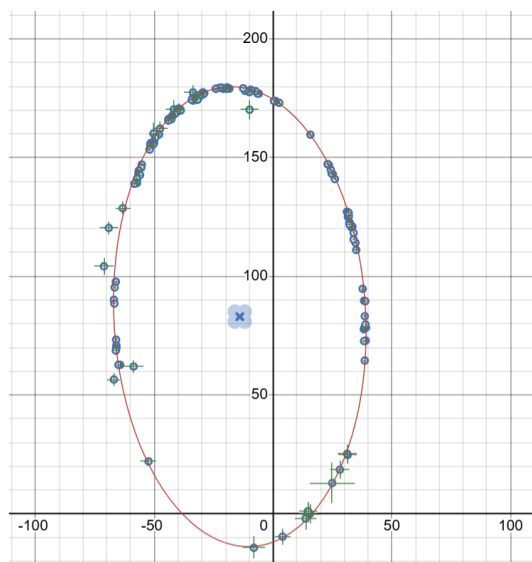


**Figure 4** Path of S2 in the sky plane modeled in Desmos with Sgr A\* at the origin with positions measured in milli-arcseconds (mas). North-up, East-right.

By identifying individual astrometric data points and comparing their timestamps, we can determine the direction of S2's orbital motion. The star covers a much larger arc near periastron, such as between 2002 and 2003, than it does near apoapsis, such as between 2012 and 2013, consistent with the expectations of Kepler's Second Law. Observations are not recorded continuously throughout each year; notably, there is a gap when the Sun passes through Sagittarius in late November to early December, rendering observations of the Galactic Center infeasible. The steady reduction in error bars over the observation period reflects improvements in the sensitivity and precision of the instruments used.

S2's nonzero Doppler velocities confirm that its orbit is not confined to the plane of the sky; instead, the orbital plane must be inclined with respect to our line of sight. The velocities are negative on the eastern side of the orbit (indicating motion toward the observer) and positive on the western side (indicating motion away). This pattern implies that the southern portion of the orbit lies farther from us, while the northern portion is closer.

According to Kepler's first law, S2 should orbit Sgr A\* in an elliptical path, with Sgr A\* at one focus of the ellipse. If the true orbit is an ellipse, then its projection onto the sky plane will also appear as an ellipse—except in the special case where the line of sight lies in the orbital plane, in which case the

projection reduces to a line segment. We verify this by fitting an ellipse to the raw astrometric data of the projected orbit in the sky plane.

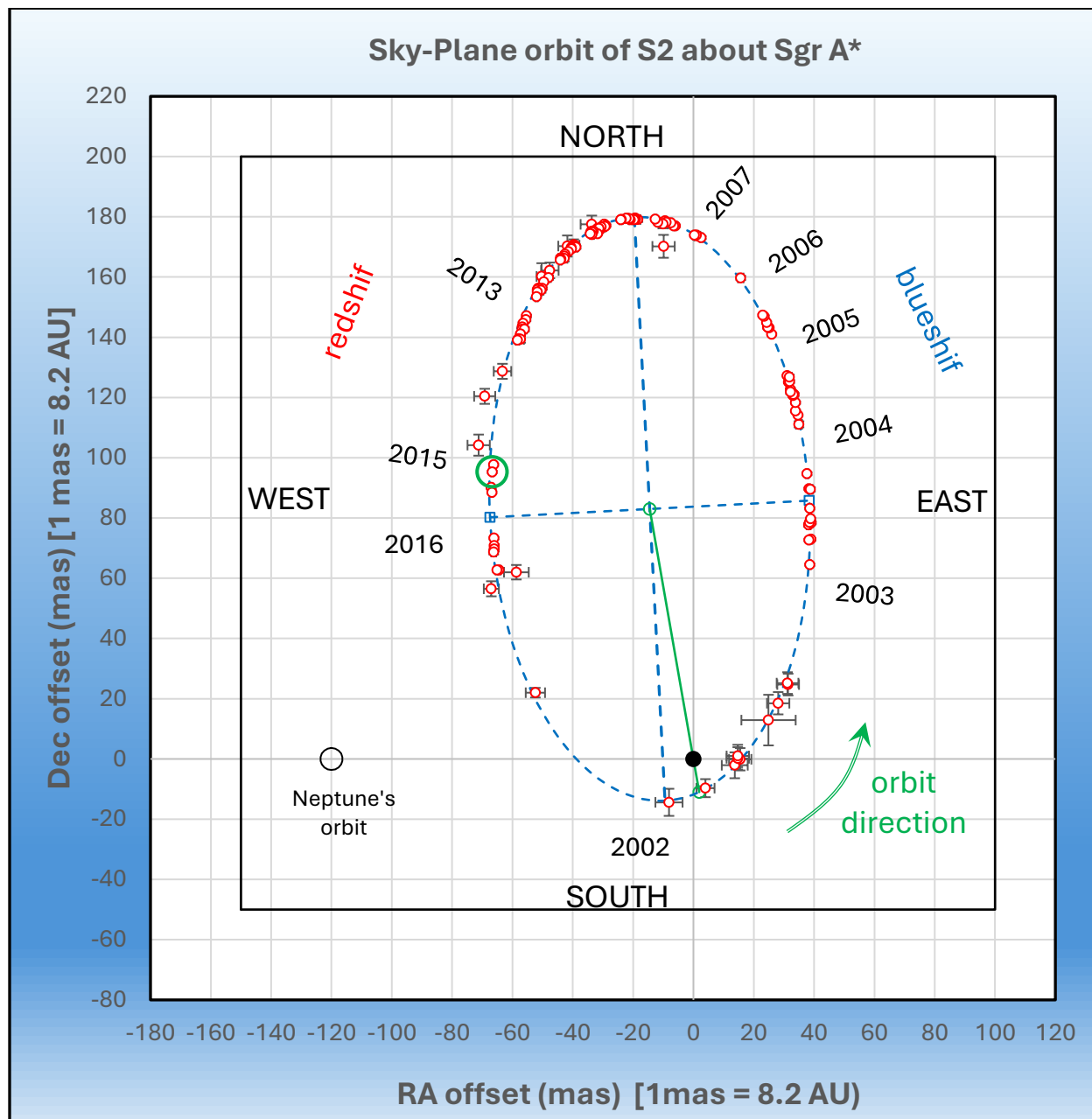


**Figure 5** Path of S2 in the sky plane modeled in Microsoft Excel with Sgr A\* at the origin with positions measured in milli-arcseconds (mas). North-up, East-right.

Fortunately, the data span more than one complete orbit, allowing for a relatively precise determination of the orbital period. One method is to track the star's position angle—defined as the angle measured

counterclockwise on the sky from due South from Sgr A\* to the position of S2. Given the sky-projected x- and y-coordinates of S2 with the origin centered on Sgr A\*, the position angle is simply:

$$\text{Position Angle} = \arctan\left(\frac{x}{-y}\right).$$

Care must be taken to resolve the correct quadrant, as the standard arctangent function is multivalued. It is preferable, therefore, to use the two-argument arctangent function, *atan2*, which handles quadrant ambiguity explicitly.

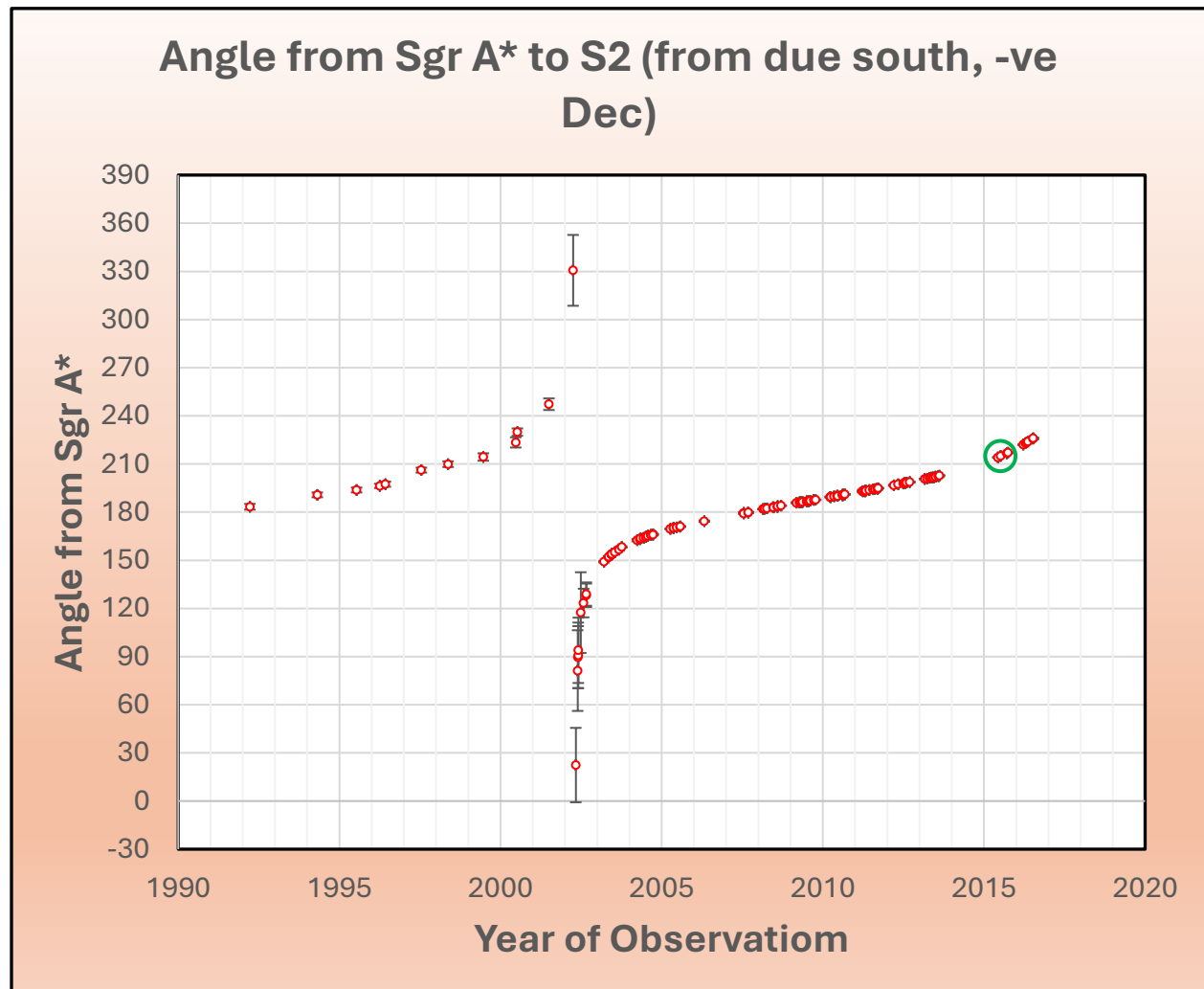


**Figure 6** Position angle of S2 measured counterclockwise on the sky from due South from Sgr A\* to the position of S2.

While the position angle itself is not astrophysically meaningful, it serves as a convenient proxy for tracking the star's motion and identifying when S2 returns to the same point in its orbit. To determine the orbital period, we plot the position angle as a function of time and compare it to a time-shifted version of the same curve (with an offset  $t + T$ , where  $T$  is the trial orbital period). We then adjust  $T$  until the two curves align, indicating a repeat in orbital phase. In this analysis, we find  $T = 16.0$  years, in excellent agreement with the professional determination reported by Gillessen et al. (2017).

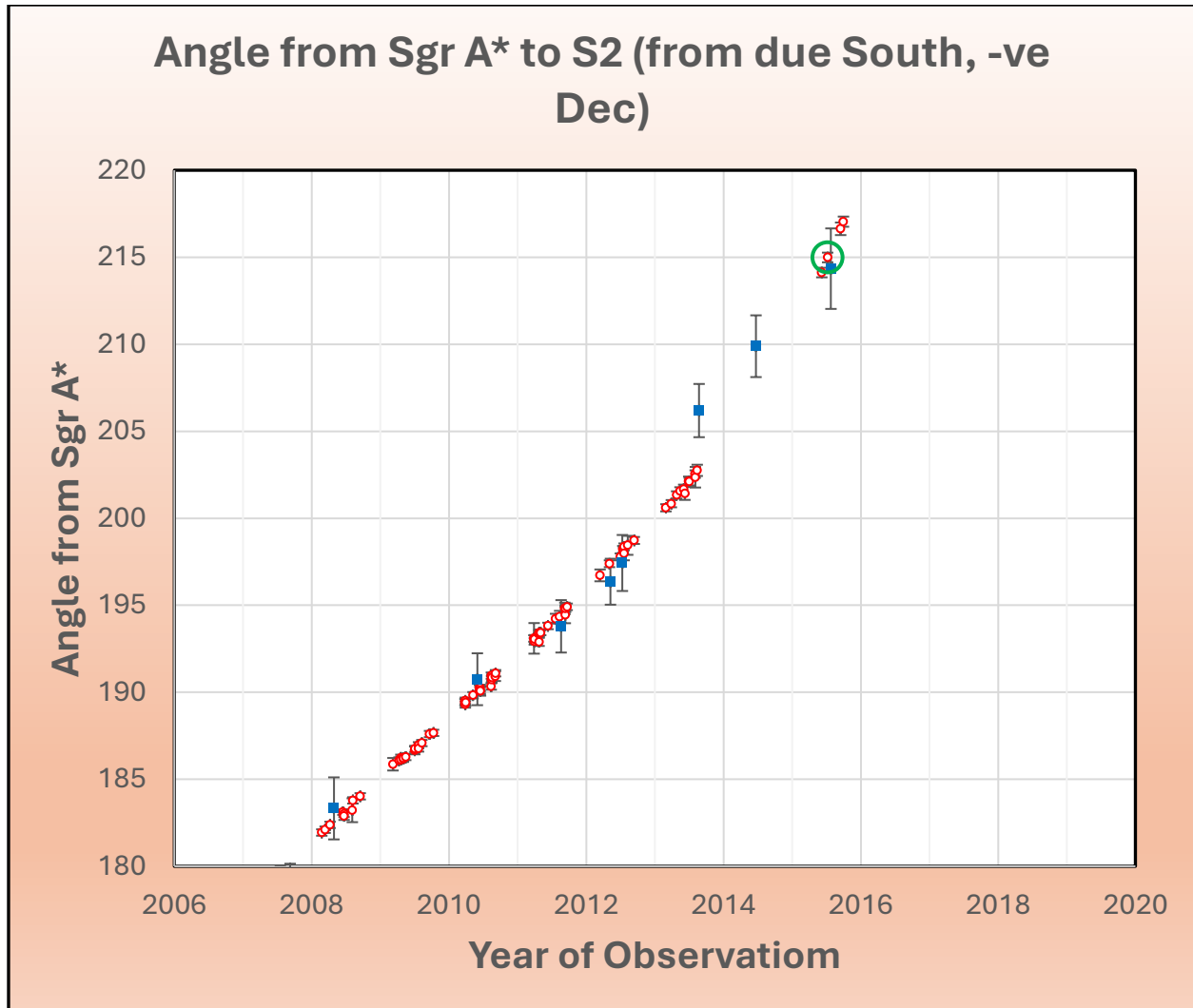


**Figure 7** Position angle of S2 as a function of time compared with a time-shifted version of the same curve.

The eccentricity of an ellipse is defined as  $e = CF/CP$ , where  $CF$  is the distance from the center to the focus, and  $CP$  is the distance from the center to periapsis. According to Kepler's first law, Sagittarius A\* must reside at one of the foci of S2's true elliptical orbit. Although the projection of this orbit onto the sky plane generally distorts the orientation—such that the foci and periapsis no longer lie along the apparent major axis—the *ratio* between the  $CF$  and  $CP$  distances is preserved under projection. This is because the projection of a straight line in three-dimensional space remains a straight line—except in the special case where the line of sight is parallel to the original line, in which case the projection reduces to a point. This geometric invariance allows us to determine the eccentricity of the true orbit directly from the projected ellipse. Since the projected coordinates of the ellipse's center and relevant focus can be identified from astrometric data in the sky plane, the key remaining task is to locate the projected position of true periapsis.

To do this, we plot a vector from the center of the ellipse in the sky plane to the origin, the location of Sgr A\*, and extend it beyond this point by a variable additional length until it just touches the ellipse at true periapsis. The magnitude of this vector gives the center to periapsis distance. The eccentricity of the true

orbit ellipse can be obtained with the ratio previously stated. Importantly, this is not equivalent to the eccentricity of the projected ellipse in the sky plane.

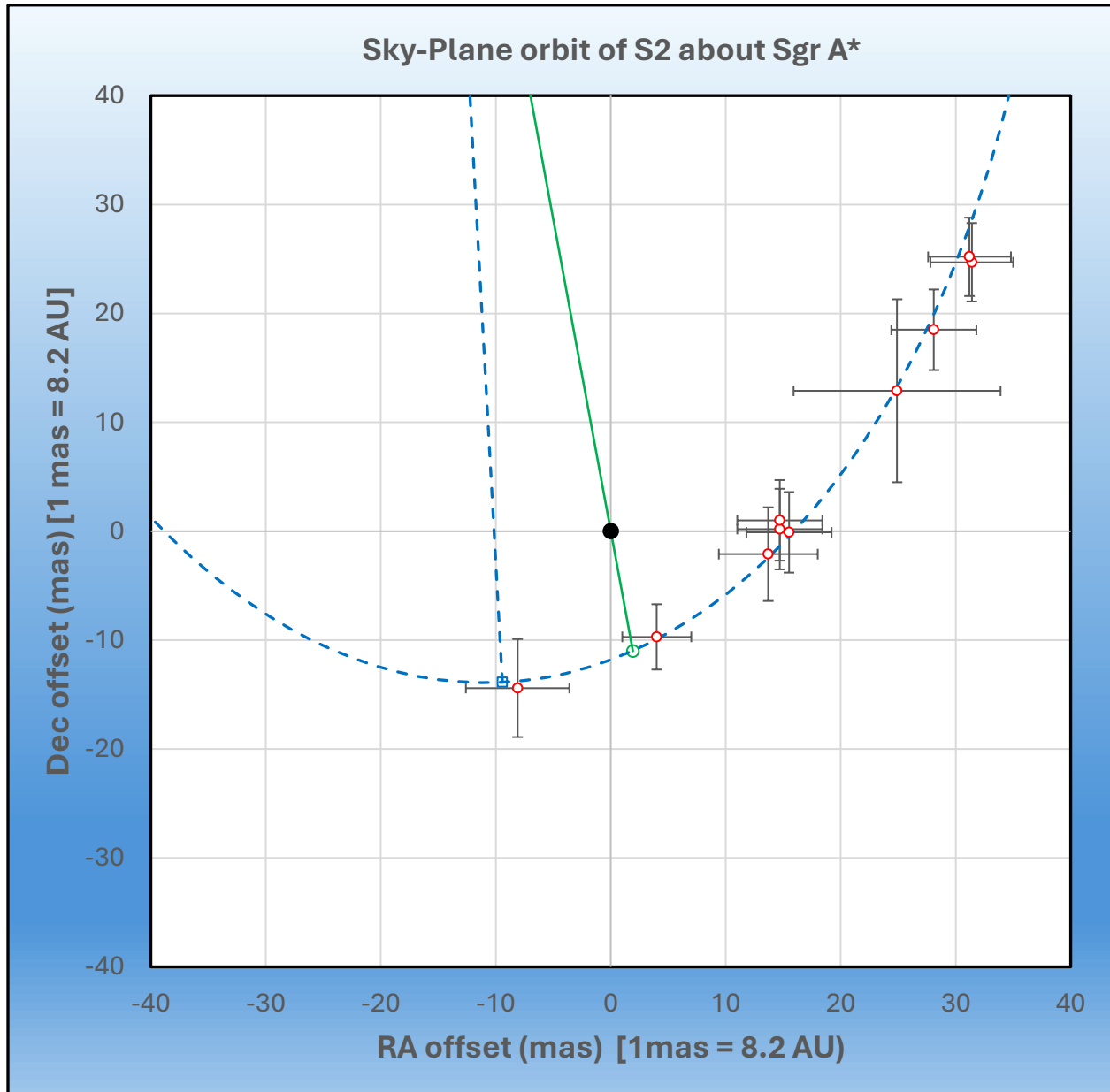


*Figure 8* Projected coordinates of the ellipse's relevant focus and periastron along the projection of the major axis of the true elliptical orbit.

### 3.2 Deprojection from the Sky Plane to the Orbit Plane

We know that the observed ellipse in the sky plane is not S2's true elliptical orbit in three-dimensional space (S2's Doppler velocities and the offset position of Sgr A\* relative to either geometric focus of the projected ellipse confirm as much). However, we know that the true orbit projects along our line of sight, the +z-direction, to generate the projected ellipse in the sky plane. Therefore, points on the true elliptical orbit in the orbit plane have the same x- and y-coordinates as their projected points on the apparent

elliptical orbit in the sky plane. The z-coordinates of all points in the sky plane are zero by definition in our coordinate system. In contrast, points on the true orbit may lie either in front of or behind this plane. Those in front on the portion of the orbit tilted toward the observer have positive z-coordinates; those behind on the portion tilted away have negative z-coordinates. To recover the full three-dimensional orbit—or “deproject” it—we must assign appropriate z-coordinates to each point on the sky-plane ellipse. This is done by rotating the projected ellipse into the orbit plane. We accomplish this by aligning the unit vector normal to the sky plane with the unit vector normal to the orbit plane and verifying that the resulting deprojected ellipse has the same eccentricity as calculated from the projected geometry using the method described previously.

The foci of an elliptical orbit lie along its major axis at a distance  $c = \sqrt{a^2 - b^2}$  from its center, where  $a$  and  $b$  are the semi-major and semi-minor axes, respectively. However, when an orbit is projected onto the sky plane, the apparent positions of the foci are generally displaced from their true locations. This displacement arises because the orbital plane is typically inclined—or “tilted”—with respect to the sky plane.

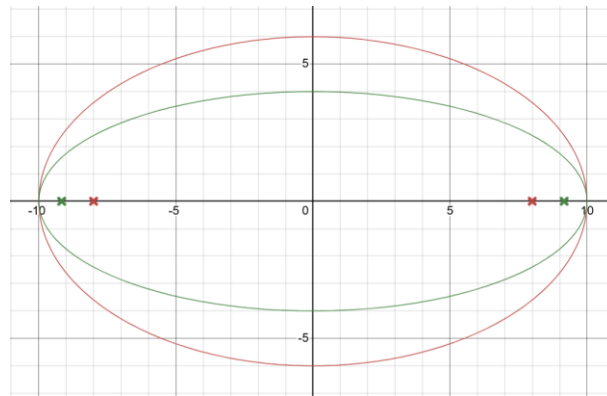


**Figure 9** Tilting an elliptical orbit (red) about its major axis (green) increases the apparent distance between the foci and the center along the projected major axis.

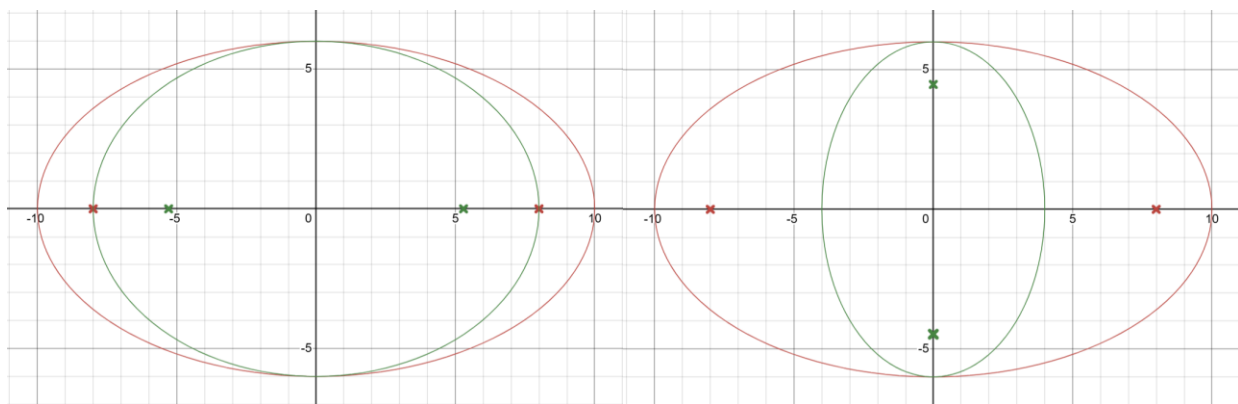


**Figure 10** Conversely, tilting the orbit (red) about its minor axis (green) reduces this separation (left) and can even shift the apparent foci onto the projected minor axis (right)—so that what appears to be the major axis in the sky-plane projection is, in fact, the true orbit’s minor axis. In both cases, when the tilt is confined to a single axis, the true foci remain aligned with one of the projected ellipse’s axes. However, when the orbit is inclined about both axes simultaneously, the projection typically displaces the true foci such that they no longer lie along either axis of the apparent ellipse.

Indeed, in the case of S2, the projected location of Sgr A\*—assumed to be at one of the true foci—is visibly offset from both axes of the best-fit ellipse in the sky plane.

To define the orbital plane, we specify a point lying within the plane—conventionally taken to be the origin—and the direction of a vector normal to the plane, known as the pole vector,  $\mathbf{n}$ . This direction is uniquely determined by two angles: the polar angle ( $\theta$ ), measured from the positive z-axis, and the azimuthal angle ( $\varphi$ ), measured counterclockwise from the +x-axis toward the +y-axis in the sky plane. Assuming the pole vector has unit magnitude and originates at the origin, its tip has the Cartesian coordinates:

$$\mathbf{n} = \begin{pmatrix} n_x \\ n_y \\ n_z \end{pmatrix} = \begin{pmatrix} \sin \theta \cos \varphi \\ \sin \theta \sin \varphi \\ \cos \theta \end{pmatrix}$$

Two key constraints allow us to determine the z-coordinates of points in the true orbit plane relative to the sky plane. First, the vector from Sgr A\* to any point on the orbit must be orthogonal to the pole vector  $\mathbf{n}$ .

$$\begin{pmatrix} n_x \\ n_y \\ n_z \end{pmatrix} \cdot \begin{pmatrix} x \\ y \\ z \end{pmatrix} = xn_x + yn_y + zn_z = 0$$

Second, each point in the true orbit shares the same x- and y-coordinates as its projected counterpart in the sky plane.

Together:

$$z = \frac{-(xn_x + yn_y)}{n_z}$$

With these constraints, we can solve for the full three-dimensional positions—x, y, and z—of all points on the deprojected ellipse, including the orbit center and periaapsis. By construction, all these reconstructed points lie within the same tilted plane. However, it is crucial to recognize that an arbitrary tilt, defined by a generic pair of angles ( $\theta$ ,  $\varphi$ ), does not necessarily yield the true orbital plane.

There are two geometric constraints that allow us to determine the specific pair of angles ( $\theta$ ,  $\varphi$ ) that define the normal vector to the true orbital plane. First, the line connecting the ellipse center, the relevant focus, and the periaapsis must lie along the major axis of the true orbital ellipse. Second, the true ellipse must have an eccentricity given by  $e = CF/CP$ , where CF and CP refer to the distances between the projections of the center, focus, and periaapsis of the true orbit in the sky plane. In practice, we iterate over different pairs of tilt angles ( $\theta$ ,  $\varphi$ ) and reconstruct the deprojected ellipse for each. We identify the correct orbit plane as the one for which the reconstructed ellipse simultaneously satisfies both conditions.

To help constrain the orientation of the true orbital plane further, we consider both the direction of orbital motion and the Doppler velocity data. The observed motion of S2 is counterclockwise in the sky plane, and the Doppler velocities are negative on the East side of the orbit. This indicates that the northern side of the orbit is closer to us, meaning it lies in front of the sky plane. Assuming we seek the orientation nearest to zero tilt, this suggests that the polar angle  $\theta$  (measured from the +z-axis) should be positive, and the azimuthal angle  $\varphi$  (measured from the +x-axis toward the +y-axis) should be negative—that is, the orbital pole vector points toward the Southeast in our coordinate system.

This choice removes a key ambiguity: for any set of tilt angles  $(\theta, \varphi)$  that defines a plane consistent with the projected ellipse and its eccentricity, the reflection  $(-\theta, -\varphi)$  defines an alternate but geometrically valid plane. However, this reflected solution implies that the northern side of the orbit lies behind the sky plane, which contradicts the observed sign of the Doppler velocities. Therefore, we safely reject the  $(-\theta, -\varphi)$  solution in favor of the one consistent with both proper motion and line-of-sight velocity data.

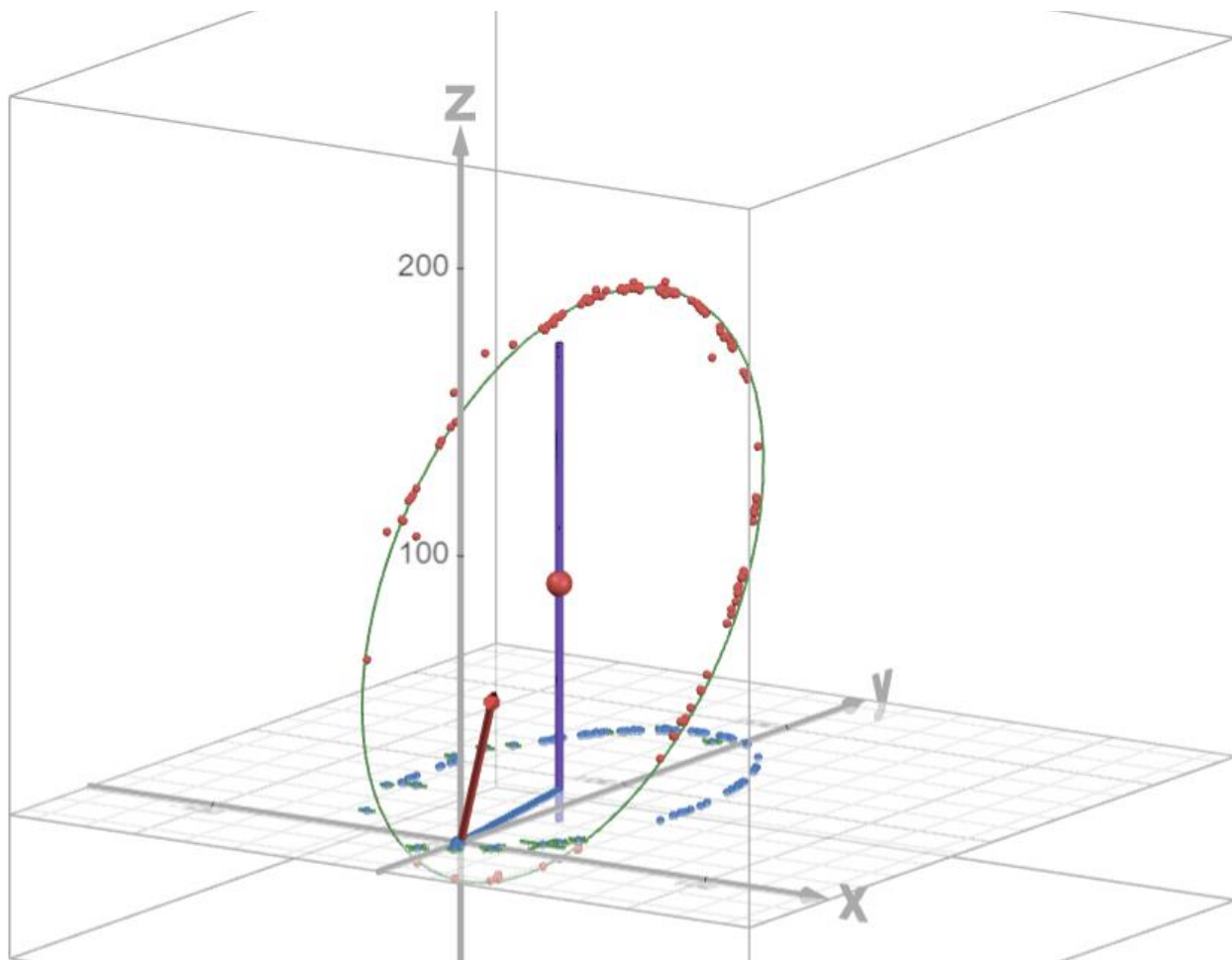


**Figure 11** Apparent orbit of S2 in the sky plane (blue points) and reconstructed true orbit in the orbital plane (red points), modeled in Desmos 3D with Sgr A\* at the origin; positions are in milli-arcseconds (mas), with North along +y and East along +x. Also shown: the center of the ellipse in the orbital plane (red sphere) and its projection along the line of sight (purple line), the vector from the ellipse center to periapsis in the sky plane (blue vector), and the orbit plane's pole vector (red vector).

To visualize the orbit in three-dimensional space after deprojection, we proceed as follows: we select a trial pair of tilt angles  $(\theta, \varphi)$ , compute the corresponding unit normal vector  $\mathbf{n} = (n_x, n_y, n_z)$ , and then calculate the  $z$ -coordinates of all observed points under the constraint that they lie in the tilted orbital plane defined by  $\mathbf{n}$ . We apply the same procedure to compute the three-dimensional positions of the ellipse center and the periapsis.

The resulting set of  $(x, y, z)$  coordinates defines an ellipse embedded in a tilted plane in three-dimensional space. This reconstructed ellipse can then be compared directly—within the same plane and coordinate

frame—to a reference ellipse having the same semi-major axis, the known eccentricity, and with Sgr A\* placed at one focus. When the trial angles ( $\theta$ ,  $\phi$ ) correctly describe the orientation of the true orbit plane, the reconstructed and reference ellipses will coincide.

Although the orbital eccentricity can be determined directly from the sky-projected geometry via projection-invariant ratios, the true value of the semi-major axis remains unknown until the correct orbital tilt is identified. The final deprojected orbit thus not only recovers the true orbital shape but also resolves its absolute spatial scale.

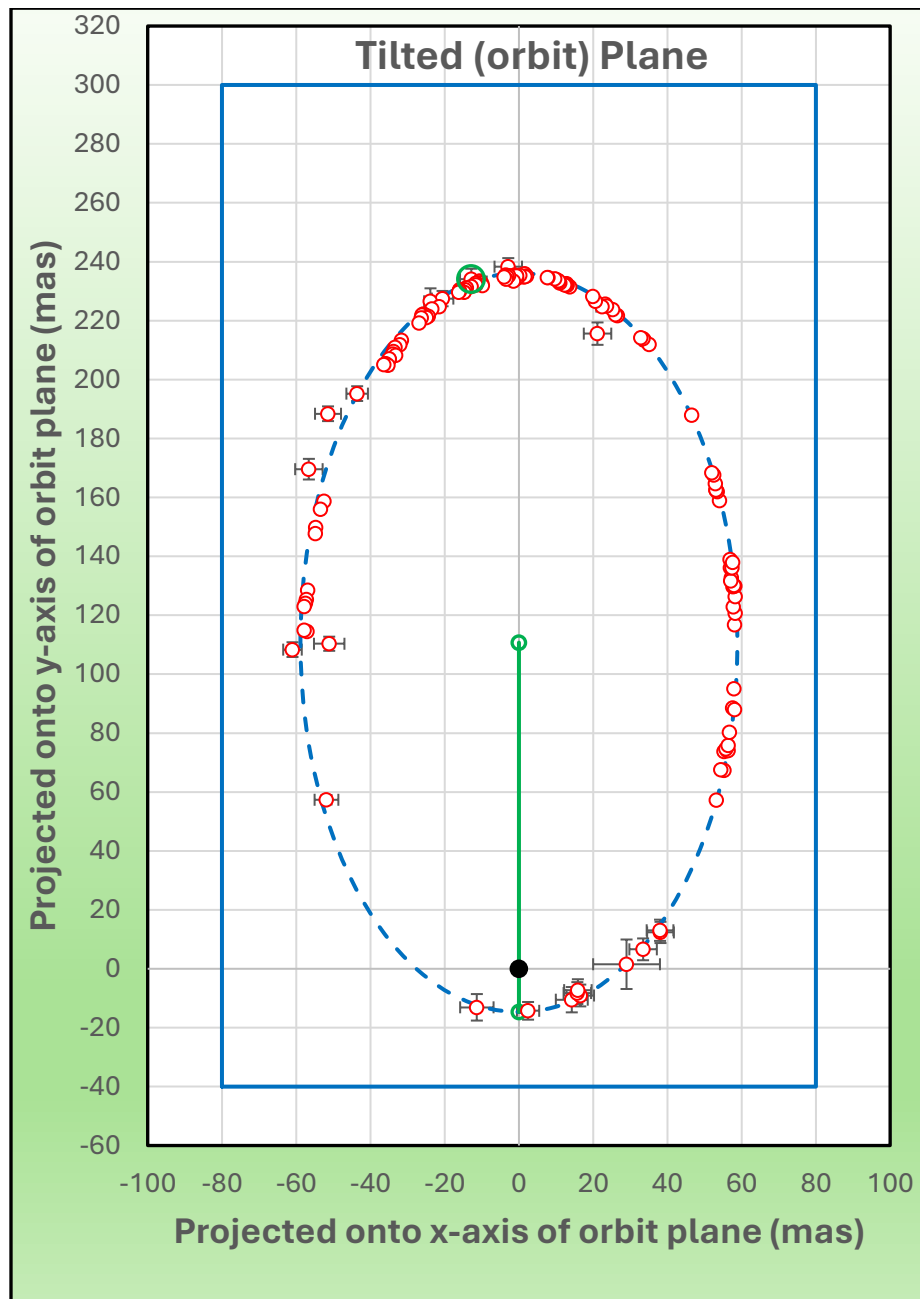


**Figure 12** Path of S2 in the orbit plane modeled in Microsoft Excel with Sgr A\* at the origin with positions measured in milli-arcseconds (*mas*).

Alternatively, the deprojected orbit can be visualized in two dimensions within its own orbital plane. To do this, we plot the ellipse such that one focus (corresponding to the location of Sgr A\*) is placed at the origin. The periapsis point is positioned directly along the -y-axis, and the geometric center of the ellipse lies along the +y-axis, ensuring that the major axis is aligned vertically.

For each point on the deprojected ellipse, we compute its radial distance from the origin and its angular position relative to the periapsis. The angle between the vector from the origin to periapsis and the vector from the origin to the given point is obtained using vector operations: the dot product yields  $\cos(\text{angle})$ , and the cross product yields  $\sin(\text{angle})$ . The sign of the sine term is determined by the direction of the z-component of the cross product, which distinguishes between clockwise and counterclockwise rotations. The final angle is computed using the two-argument arctangent function,  $\text{atan2}(\sin(\text{angle}), \cos(\text{angle}))$ , ensuring the angle lies in the correct quadrant.

When the correct tilt angles ( $\theta, \phi$ ) are used, the resulting plot matches a reference ellipse with the same semi-major axis length, the known eccentricity, and a focus located at the origin. This representation captures the true shape of the orbit in its intrinsic two-dimensional plane.

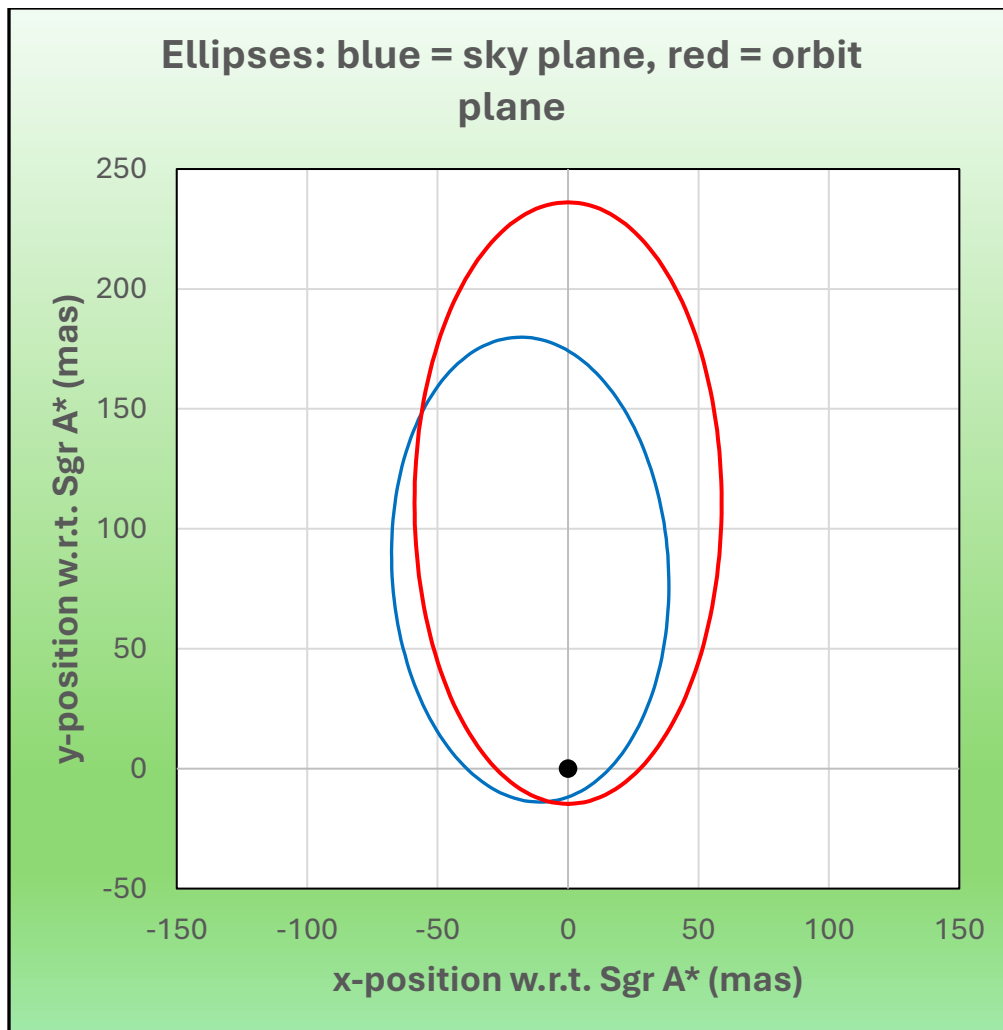


Figure 13 Apparent orbit of S2 in the sky plane (blue) and reconstructed true orbit in the orbital plane (red), modeled in Microsoft Excel with Sgr A\* at the origin and positions measured in milli-arcseconds (mas).

### 3.3 Doppler Velocities Confirm Orbit Solution and Distance to Galactic Center

Doppler velocity measurements provide an essential constraint on the true three-dimensional orbit of S2. Since our line of sight corresponds to the +z-axis in the adopted coordinate system, the line-of-sight velocity is directly related to the time derivative of the z-coordinate of the star's position.

To determine this component, we first plot the deprojected z-coordinate of S2 as a function of time. By fitting a fourth-order polynomial to this time series and analytically differentiating the fit, we obtain an estimate of the line-of-sight velocity,  $dz/dt$ , at each epoch. To convert these values from angular units (mas/yr) to physical units (km/s), we require an assumed distance to the Galactic Center,  $R_0$ , which we treat as a free parameter. We then compare these predicted velocities with the observed Doppler shifts, adjusting  $R_0$  to achieve the best match.

The model shows excellent agreement with the data for values of  $R_0$  in the range 7.8–8.6 kpc, consistent with recent high-precision measurements. This correspondence between predicted and observed line-of-sight velocities provides strong validation of the orbit reconstruction and confirms that the deprojected orbit plane and tilt angles are consistent with both astrometric and spectroscopic constraints.

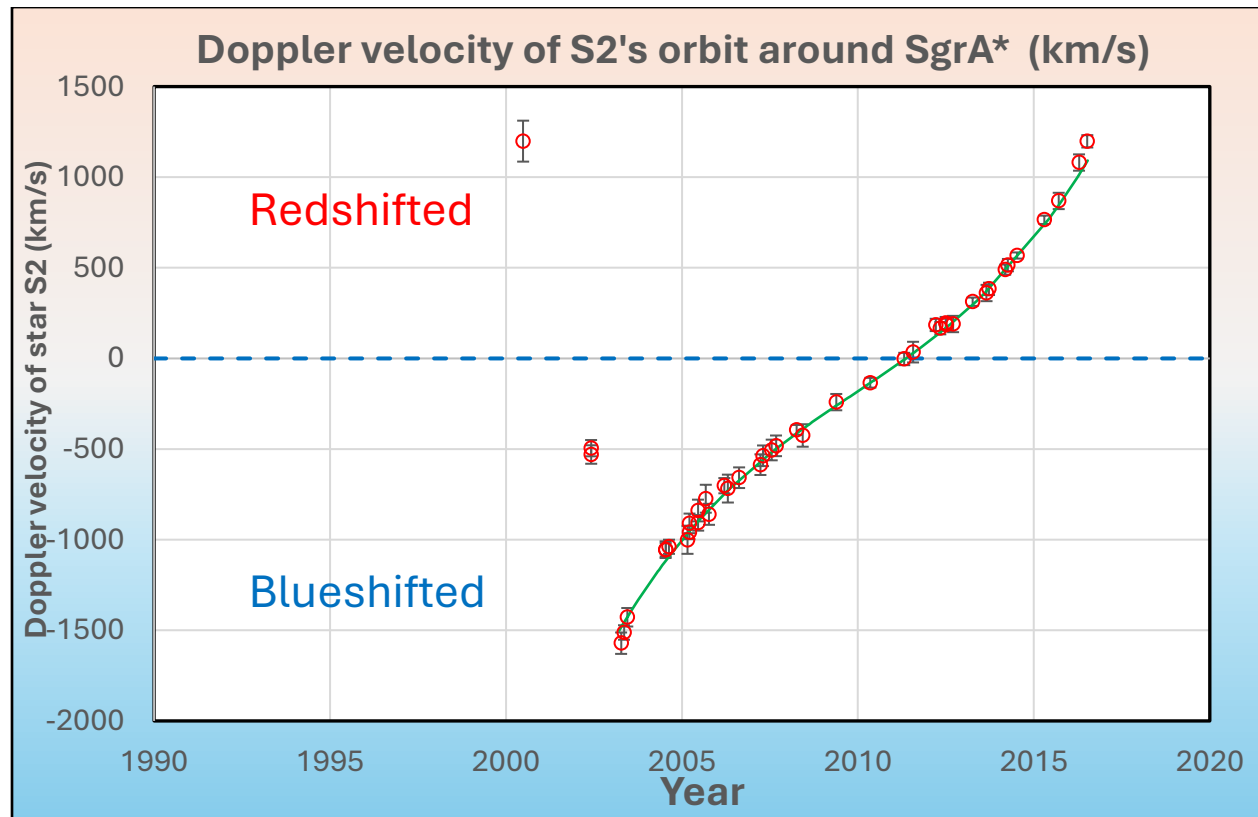


**Figure 14** Line-of-sight radial velocities of S2 derived from Doppler shifts (data points) compared with predicted velocities based on changes in the z-coordinate from deprojected orbital motion (green line).

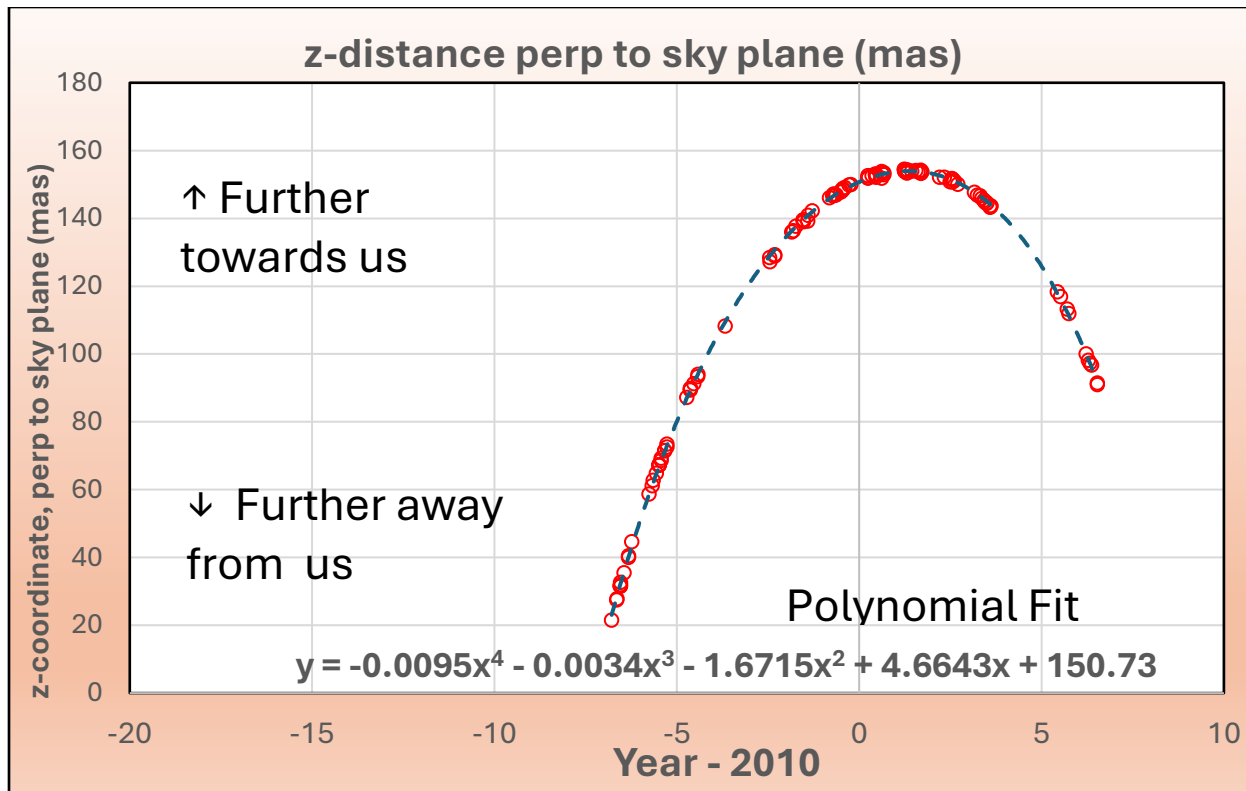


*Figure 15 Fourth-order polynomial fit of the z-coordinate perpendicular to the sky plane.*

### 3.4 Classical Orbital Elements

A Keplerian orbit is fully characterized by six classical orbital elements in addition to the orbital period: the semi-major axis ( $a$ ), eccentricity ( $e$ ), inclination ( $i$ ), longitude of the ascending node ( $\Omega$ ), argument of periapsis ( $\omega$ ), and time of periapsis passage ( $T_p$ ). From our modeling, we have already determined four of these:  $a$ ,  $e$ ,  $T$ , and  $T_p$ . The remaining three describe the orientation of the orbit in three-dimensional space, relative to the plane of the sky and a reference direction, taken here as celestial North.

The inclination is the angle between the orbital plane and the sky plane (defined as the  $x$ - $y$  plane in our coordinate system). More precisely, it is the angle between the true orbit's pole vector and the apparent orbit's pole vector (defined as the  $+z$ -axis in our coordinate system). By convention, inclination ranges from  $0^\circ$  to  $180^\circ$ , where values between  $0^\circ$  and  $90^\circ$  correspond to prograde orbits (motion in the direction of increasing position angle, North through East), and values between  $90^\circ$  and  $180^\circ$  correspond to retrograde orbits (motion opposite this direction). In our case, S2's orbit is retrograde. The polar angle of the orbit pole from our best-fit deprojection is  $\theta = 45.4^\circ$ , so the inclination is conventionally expressed as  $i = 180^\circ - \theta = 134.6^\circ$ .

The longitude of the ascending node specifies the position angle (measured from North through East) of the ascending node—the point where the star crosses the sky plane moving away from the observer. In our coordinate system, the azimuthal angle  $\varphi$  defines the rotation of the orbital plane's pole from the  $+x$ -axis toward the  $+y$ -axis. The azimuthal angle from our best-fit deprojection is  $\varphi = -47.3^\circ$ . Therefore, to convert our azimuthal angle into the conventional longitude of the ascending node, we apply  $\Omega = 180 - \varphi = 227.3^\circ$  by convention.

The argument of periapsis is the angle within the orbital plane from the ascending node to periapsis, measured in the direction of motion. This value is obtained directly from our geometric reconstruction of the deprojected orbit, yielding  $\omega = 65.7^\circ$  in our best-fit model.

	Classical Orbital Elements						
	a	e	inc	Omega AN	Long-peri	T-peri	T period
This Work:	125.4	0.883	134.6	227.3	65.7	2002.32	16.1
Target:	125.5	0.884	134.2	226.9	65.5	2002.33	16.0

**Figure 16** Comparison with published orbital parameters (Gillessen et al. 2017) demonstrates that the deprojection method accurately reconstructs the true three-dimensional orbit.

## IV. Keplerian Analysis and Mass Estimation of Sgr A\*

### 4.1 Kepler's Law of Equal Areas

So far, only the projected geometry of the orbit in the sky plane has been used to infer the true orbit's shape and orientation. However, if the underlying orbit is indeed Keplerian, then its dynamical behavior must also conform to Kepler's Second Law—the Law of Equal Areas—which states that a line connecting the orbiting body to the central mass sweeps out equal areas in equal times. In other words, the area swept out by the vector from Sgr A\* to S2 should increase linearly with time. Consequently, a plot of swept area versus time should yield a straight line, whose slope corresponds to the total area of the true orbital ellipse divided by its period.

To calculate the area swept out by S2 as it orbits Sgr A\*, we begin by constructing a reference circle of radius equal to the semi-major axis,  $a$ . For each observational point, we determine the angle  $\beta$  in degrees at the center of this circle between the major axis and the projection of the point onto the circle along the x-axis. The area swept is then approximated as:

$$Area_{swept} = \frac{\beta}{360^\circ} \pi a^2 \cdot \frac{\beta}{a} \pm \frac{1}{2} e a x$$

where the correction term  $\frac{1}{2} e a x$  accounts for the area of the triangle formed by the focus, the center, and the instantaneous position of S2. This correction is subtracted when  $\beta < 180^\circ$  and added when  $\beta > 180^\circ$ , ensuring the correct directional sense of area accumulation.

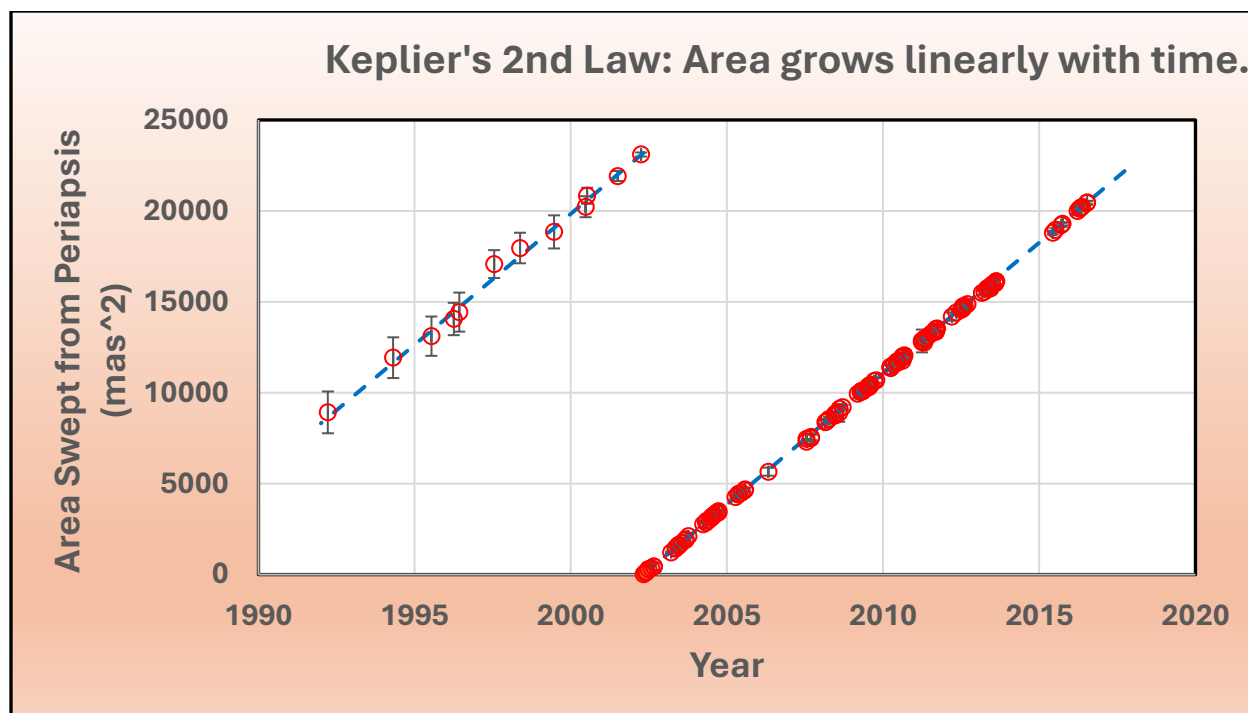


*Figure 17* Cumulative area swept out by S2 as it orbits Sgr A\*.

A plot of swept area versus time yields an excellent linear relationship, confirming that the motion obeys Kepler's Second Law. Notably, deviations from the best-fit orbital orientation (i.e., incorrect choices of tilt angles  $\theta$  and  $\varphi$ ) result in visibly non-linear plots. From the linear fit, we can also determine the time of periaapsis passage, and overlaying the theoretical line provides an excellent match to the data.

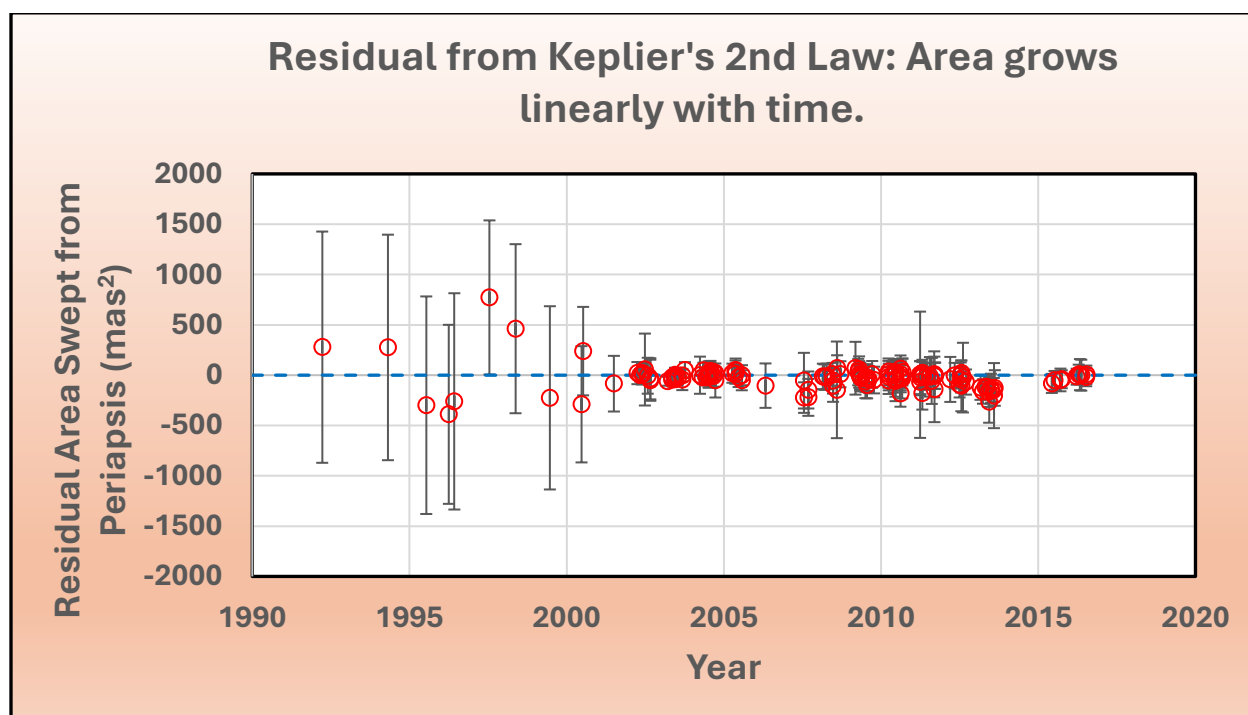


*Figure 18* Residual area swept from periaapsis by S2 as it orbits Sgr A\*.

A plot of residuals shows no significant systematic deviations, supporting the conclusion that the deprojected orbit is Keplerian to within observational error.

#### 4.2 Estimate of the Mass of Sgr A\*

With the true semi-major axis,  $a$  (in astronomical units), and the orbital period,  $T$  (in years), we can calculate the mass of Sgr A\* using Kepler's Third Law:

$$M = \frac{a_{au}^3}{T_{yr}^2} M_{sun} = 4.22E6 M_{sun}$$

This estimate agrees well with the accepted value of  $(4.28 \pm 0.10) \times 10^6 M_{sun}$  reported in Gillessen et al. (2017), confirming the consistency of our deprojection method with established dynamical mass measurements of the central black hole.

## V. Discussion

### 5.1 Lessons for Students

Beyond the core scientific goals of this project, an equally important objective is to foster in students a sense of intellectual wonder—an appreciation for the profound and often counterintuitive truths that emerge from a careful study of our universe. Engaging directly with real astronomical data, students are invited not merely to perform calculations, but to encounter, through hands-on inquiry, the extraordinary reality that a single star, tracing its arc across the sky, can reveal the presence of a supermassive black hole and test the predictions of general relativity.

To accommodate learners at a wide range of levels, the project includes two versions of the orbital deprojection method—each with distinct pedagogical benefits. The Desmos implementation emphasizes conceptual clarity and accessibility. It relies on an interactive slider-based interface in which students manipulate eight key parameters: the x- and y-coordinates of the orbit's center in the sky plane, the semi-major and semi-minor axes of the projected ellipse, the rotation angle of the ellipse in the sky plane, the polar angle ( $\theta$ ) and azimuthal angle ( $\varphi$ ) of the orbital plane's orientation, and the true eccentricity of the orbit. This interface requires no prior experience with astronomy or programming, making it suitable for learners as early as middle school while still providing meaningful insight into orbital geometry and projection effects.

For students seeking greater analytical rigor, the Excel-based version of the project offers expanded opportunities for precision, iteration, and exploration. By working directly with numerical data and formulas, students can gain deeper experience in curve fitting, coordinate transformations, and the application of Kepler's laws. This environment also enables more precise comparisons between model predictions and observed data, encouraging the development of quantitative reasoning and data literacy.

### 5.2 Improvements

While the methods used in this project rely on Newtonian orbital mechanics, it is important to recognize that the true motion of stars in the strong gravitational field near a supermassive black hole is governed by general relativity. One of the most striking consequences of this revised framework is the relativistic precession of orbital periastron: for an object on an eccentric orbit passing close to a massive body, the

point of closest approach does not remain fixed but advances in angle with each orbit. This prograde shift in the periapsis—first famously observed in the orbit of Mercury—is a hallmark prediction of general relativity.

In our present analysis, based on the astrometric and radial velocity data available for the star S2 through 2016, the relativistic precession is not yet visible. The limited precision and temporal coverage of the first full orbit of S2, especially when derived using simpler deprojection techniques, precludes the detection of this subtle effect. However, more recent studies have now succeeded in confirming relativistic precession with high statistical significance. This breakthrough has been made possible by the GRAVITY instrument, an optical interferometer operating at the Very Large Telescope Interferometer (VLTI), which combines light from four telescopes (and occasionally a fifth) to achieve exquisite angular resolution and astrometric precision on the order of tens of microarcseconds.

The incorporation of GRAVITY data represents a major leap forward in our ability to test general relativity in the strong-field regime and to refine measurements of the S2 orbit and the mass distribution near Sgr A\*. While our current project does not include this new data, it points the way forward: future iterations could be expanded to incorporate GRAVITY observations or generalized to analyze additional stars in the S-cluster.

## VI. Conclusion

Working on this project has been transformative. I came to it with the goal of building a toolset—technical, analytical, and computational—that could help make the frontier of astronomy more accessible to students. I leave it not only with those tools sharpened but with a deeper, more personal connection to the cosmos itself. Modeling the orbit of S2 has made the distant and abstract feel near and concrete. The center of the Milky Way is a region we can never visit directly—hidden behind clouds of interstellar dust, bathed in ionizing radiation, and anchored by a supermassive black hole that warps space and time, but through the process of recreating S2's path—deprojecting it from the sky plane, fitting it with ellipses, estimating orbital elements, and applying Kepler's laws—we inhabit the dynamics of the system ourselves. It becomes real in a way that data tables alone cannot achieve. The mathematics is not just a tool of analysis, but a bridge to presence.

Pedagogically, this project taught me the power and challenge of communicating technical methods in a way that is both accurate and intuitive. Designing the Desmos-based orbit deprojection for students required me to distill complex concepts—coordinate transformations, orbital mechanics, projection geometry—into visual, hands-on forms. In contrast, the Excel-based analysis was an opportunity to offer more depth to upper-level students, showing how observational data is transformed into physical insight. Across both versions, I learned that clarity in science communication does not mean oversimplification. Rather, it means building scaffolding—both conceptual and visual—that helps students climb from the familiar into the extraordinary.

## Bibliography

- [1] Beletsky, Y. 2011, in Encyclopædia Britannica, *Very Large Telescope*, <https://www.britannica.com/topic/Very-Large-Telescope#/media/1/753079/164803>
- [2] European Southern Observatory (ESO) 2002, NAOS-CONICA Adaptive Optics System on the VLT, photograph, <https://www.eso.org/public/belgium-fr/images/vlt-naos-conica1/>
- [3] European Southern Observatory (ESO) 2004, *SINFONI Instrument in the Laboratory*, <https://www.eso.org/public/belgium-fr/images/sinfoni-int-lab-hq2-03-04/>
- [4] Gillessen, S., Plewa, P. M., Eisenhauer, F., et al. 2017, ApJ, 837, 30. <https://doi.org/10.3847/1538-4357/aa5c41>
- [5] Nobel Committee for Physics 2020, Scientific Background on the Nobel Prize in Physics 2020: Theoretical foundation for black holes and the supermassive compact object at the galactic centre, NobelPrize.org, <https://www.nobelprize.org/uploads/2020/10/advanced-physicsprize2020.pdf>